Journal of GeoEngineering, Vol. 12, No. 1, pp. 35-43, March 2017
http://dx.doi.org/10.6310/jog.2017.12(1).4

ANALYSIS OF PILE BEHAVIOR IN LIQUEFIABLE SEABED SAND WITH *p-y* CURVE APPROACH

Sheng-Huoo Ni [1*], Kuo-Chi Huang [2], Zong-Wei Feng [3], Chung-Hsuan Fan [2], and Siao-Pei Su [2]

ABSTRACT

This study focuses on the case study of Changhua offshore wind farm with using two different models to simulate the behavior of soil-pile interaction of liquefiable seabed sand. Two ways are used to modify the *p-y* curve due to excess pore water pressure induced by seismic vibration. They are Liu and Dobry method and Chang and Hutchinson method. These two methods enable a more reasonable assessment of pile-soil interaction in the liquefiable seabed sand under the various level of weakening effect excited by excess pore water pressure using different modified *p-y* curves. According to results analyzed, using Chang and Hutchinson method is essentially more reasonable. However, using Chang and Hutchinson method will overestimate soil resistance as r_u less than 0.2. Therefore, the Liu and Dobry method is suggested to modify the *p-y* curve as r_u less than 0.2. Also, the effect of diameter of the pile on the behavior of pile is studied and discussed.

Key words: Pile, soil liquefaction, *p-y* curve, excess pore water pressure.

1. INTRODUCTION

In recent years, energy conservation, carbon emission reduction, and the development of renewable energy have been the focuses of our government, and wind power is considered to be one of the most important sources of renewable energy. Currently, all the wind energy is generated from onshore wind farms. However, due to the limited terrain of Taiwan, the government had planned a precursor offshore wind farm at the western sea of Fang-Yuan County, Chang-Hua.

Typically, pile structure is selected for offshore wind farms with water depth less than 30 meters. Western offshore wind turbine design regulations, such as DNV-OS-J101 (2013) from Det Norske Veritas, IEC61400-3 (2009) from International Electro Technical Commission, and API RP 2A-WSD (2005) from American Petroleum Institute, are major regulations used to design wind turbine pile foundations. *p-y* curve approach is the most often used method for analyzing bearing capacity and deformation of pile foundations under lateral external loads.

Offshore wind turbine pile foundations are installed mostly in saturated soft sand layers, which have the potential of suffering from earthquake-induced soil liquefaction (Ni *et al*. 2014). Taiwan is located on tectonic plate boundary earthquake zone, they lack the consideration of the effects of soil liquefaction on pile foundation in the above regulations. Japan Road Association (JRA 1996) considers the effect of soil liquefaction on ultimate strength reduction factor with liquefaction potential index (LPI). However, the LPI is calculated by the zone of soil liquefied only. This study will discuss the moment of pile body to *p-y* curves before and after soil liquefied and pile lateral deformation. The relationship between *p-y* curves under different excess pore water pressure ratio r_u and pile lateral deformation is also discussed.

Manuscript received July 25, 2016; revised January 12, 2017; accepted January 12, 2017.
[1] Professor (corresponding author), Department of Civil Engineering, National Cheng Kung University, Taiwan. (e-mail: tonyni@mail.ncku.edu.tw).
[2] Graduate Student, Department of Civil Engineering, National Cheng Kung University, Taiwan.
[3] Projects Engineering Manager, ODE Ltd., Taiwan.

2. THEORETICAL BACKGROUND

P-y curve method is an analytical mode that analyzes a pile under lateral loading and is also the most popular method used in practical practice. The concept of Winkler model is applied in this method, which simulates the surrounding soil with numbers of springs. These springs in different depths are isolated and possess their own load-deformation curves or so-called *p-y* curves.

In the case of this study, the uppermost sand layer controls the whole pile behavior. The *p-y* curve of sand and the liquefiable sand layer is described in details below.

2.1 API *p-y* Curve of Sand

Currently, the most popular *p-y* curve of sand is the hyperbolic tangent model purposed by Murchison and O'Neill (1984) and suggested by American Petroleum Institute (API 2005). The following two equations can be used to determine the maximum soil reaction force per unit length. Equation (1) determines the maximum lateral resistance of the shallower soil, and Eq. (2) for the deeper soil. The smaller of the two is then the ultimate resistance p_u for the conservative consideration.

$$p_{us} = (C_1 z + C_2 D)\,\gamma' z \tag{1}$$

$$p_{ud} = C_3 D \gamma' z \tag{2}$$

where D is pile diameter (m),
γ' is effective unit weight of soil (kN/m^3),
z is the depth (m),
C_1、C_2、C_3 are dimensionless coefficients.

Finally, the relationship between soil reaction force p and deformation y at a specific depth can be represented by Eq. (3):

$$p = A_1 p_u \tanh\left(\frac{kz}{A_1 p_u} y\right) \tag{3}$$

where k is the subgrade reaction coefficient,

A_1 is the ultimate bearing capacity adjustment coefficient. It is obtained from the testing results of pile load tests with different pile head loading conditions.

Considering statistic loading condition:

$$A_1 = \left(3.0 - 0.8\frac{z}{D}\right) \geq 0.9$$

Considering cyclic loading condition: $A_1 = 0.9$

2.2 Reese *p-y* Curve of Sand

A series of full-scale tests had been performed by Reese *et al.* (1974) in the saturated sand at Mustang Island, USA. According to the testing results, different from the *p-y* curve of sand suggested by API, which consist of only one function, the *p-y* curve is consists of three straight sections and a parabola section (as shown in Fig. 1): initial straight line section (*o-k*); parabola connection section (*k-m*); straight line connection section (*m-u*); and ultimate strength horizontal section.

In Reese *p-y* curve of sand, the evaluation of lateral ultimate soil resistance is based on the types of soil failure mode. Two theoretical equations were proposed to calculate ultimate soil resistance at a specific depth:

$$p_{ult} = \gamma' x \left[\begin{array}{l} \dfrac{K_0 x \tan\phi \sin\beta}{\tan(\beta-\phi)\cos\alpha} \\ +\dfrac{\tan\beta}{\tan(\beta-\phi)}(D + x\tan\beta\tan\alpha) \\ +K_0 x \tan\beta(\tan\phi\sin\beta - \tan\alpha - K_a D) \end{array}\right] \tag{4a}$$

$$p_{ult} = \gamma' x\left[K_a D(\tan^8\beta - 1) + K_0 D\tan\phi\tan^4\beta\right] \tag{4b}$$

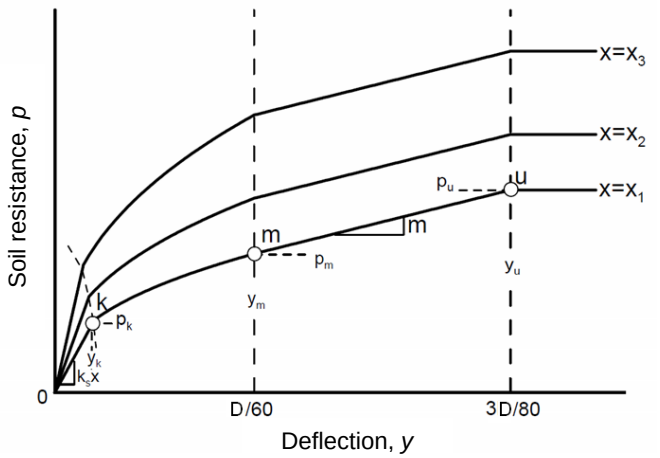

Fig. 1 Reese's *p-y* curve of sand

where ϕ is the internal friction angle of soil,

γ' is the effective unit weight,

K_o is the coefficient of static lateral earth pressure, Reese suggested that

$K_o = 0.4$,

K_a is the Rankine coefficient of active earth pressure,

x is depth,

$$\alpha = \frac{\phi}{2} \quad , \quad \beta = 45° + \frac{\phi}{2}$$

p_{ult}, obtaining from Eq. (4a), is the ultimate soil resistance of wedge failure mode in shallow soil layers, and p_{ult}, obtaining from Eq. (4b), is the ultimate soil resistance of sliding failure mode in deep soil layers. The smaller of the two is then selected to be the theoretical ultimate sand soil resistance.

After obtaining the theoretical ultimate soil resistance using Eq. (4), the following steps were employed to complete the *p-y* curve:

(1) Construct the initial straight line section using Eq. (5):

$$p = (kx)y \tag{5}$$

where x is the depth below ground surface,

k is the coefficient of soil subgrade reaction.

(2) Determine the point u:

$$(p_u, y_u) = \left(\bar{A}p_{ult}, \frac{3D}{80}\right) \tag{6}$$

Different modifying coefficient $\bar{A}$ is used with different loading types.

(3) Determine the point m

$$\left(p_m, y_m\right) = \left(Bp_{ult}, \frac{D}{60}\right) \tag{7}$$

Different modifying coefficient B is used with different loading types.

(4) After defining point m and u, the line connecting the two point is then the straight line connection section (*m-u*).

(5) A parabola (*k-m*) is then fit between origin and point m. The slope of the tangent of point m is made equal to the slope of the straight line (*m-u*). The relationship between point k and point m can be determined by Eq. (8). Coefficient n can be determined from the geometry relationship between m and u.

$$p = p_m\left(\frac{y}{y_m}\right)^{\frac{1}{n}} \tag{8}$$

In order to satisfy the continuity of geometry, n can be determined by the following equation

$$n = \frac{p_m}{y_m} \times \frac{y_u - y_m}{p_u - p_m}$$

2.3 Rollins *p-y* Curve of Liquefied Sand

A full-scale pile test was performed by Rollins *et al*. (2005) at Treasure Island, California, USA. By detonating dynamites, excess pore water pressure was excited and soil was liquefied. A concave-up *p-y* curve was then back-calculated from data obtained from strain gages installed on pile body.

This concave-up *p-y* curve was the hysteresis loop resulted from the force applied by brakes and pile head deflection. It can be seen that in the beginning of cyclic loading, as numbers of cycles increased, the hysteresis loops gradually flatten. It means that the stiffness of soil was gradually decreased, until it stabilized at the 10th cycle. The residual strength was reached at this 10th cycle and was considered completely liquefied. The *p-y* curve of this 10th cycle was then back-calculated. The relationship between soil reaction force *p* and deformation *y* is shown below.

$$p = P_d A (By)^C \tag{9}$$

Among them, $A = 3 \times 10^{-7} (z+1)^{6.05}$

$B = 2.80 (z+1)^{0.11}$

$C = 2.85 (z+1)^{-0.41}$

$P_d = 3.81 \ln |D| + 5.6$

z is the depth (m),

P_d is unitless pile diameter affection coefficient.

Since this function was derived from the in-situ test performed by Rollins *et al*. there are limitations to Eq. (9) above:

(1) The relative density of soil has to be between 40% ~ 55%.

(2) Soil lateral resistance must be less than 15 kN/m.

(3) The lateral deformation pile must be less than 150 mm.

(4) Water level must be higher, or close to, ground level.

(5) Soil depth must be less than 6 m.

2.4 Liu and Dobry Modifying Method

Different from using the traditional method of determining the relationship between $(N_1)_{60}$ of soil sample and soil strength reduction after liquefaction, Liu and Dobry (1995) performed a series of centrifuge tests to determine the trend of soil strength reduction under a different level of soil liquefaction. It is done by excited different excess pore water pressure in the sand soil samples. A linear decreasing relationship was found between excess pore water pressure ratio r_u and soil strength reduction factor C_u by regression analysis from a large amount of test data (as shown in Fig. 2):

$$C_u = 1 - r_u \tag{10}$$

Liu and Dobry (1995) suggested that, in order to simulate sand soil strength reduction after liquefaction, traditional non-liquefied *p-y* curve, for example, sand *p-y* curves proposed by Reese *et al*. (1974), can be selected as the base. C_u factors under different excess pore water pressure ratio calculated using Eq. (10) and reduced ultimate soil resistance (*p*) were also taking into account:

$$p = p_y \times C_u \tag{11}$$

where p_y is the ultimate soil resistance of the non-liquefied sand *p-y* curve.

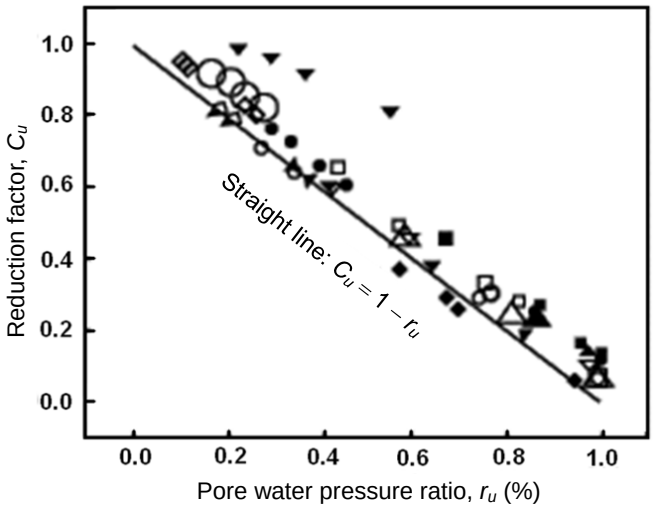

Fig. 2 Relationship between C_u and r_u (redrawn from Liu and Dobry 1995)

When r_u = 1.0, the C_u calculated from Eq. (10) is zero. However, in practical practice, it is believed that residual strength still exists after the soil was liquefied, the value C_u = 0.1 is given in such cases.

2.5 Chang and Hutchinson Modifying Method

Chang and Hutchinson (2013) studied the *p-y* curves under different excess pore water pressure ratios using modeled tests with layered soil box of length 3.9 m, width 1.8 m, and height 1.9 m. A shaking table was used to generate different earthquake signals to excite different excess pore water pressure.

Chang and Hutchinson (2013) discovered that *p-y* curves concave up as excess pore water pressure increased, which matches the full-scaled testing results of Rollins *et al*. (2005). Therefore, the *p-y* curve of Rollins *et al*. (2005), which is Eq. (9), was used as the base equation. Along with Eq. (12), the soil resistance was multiplied by the reciprocal of C_{ru} to enlarge the strength *p* of completely liquefied sand:

$$p = p_R \times \frac{1}{C_{ru}} \tag{12}$$

$$y = y_R \times C_{ru} \tag{13}$$

where C_{ru} is the excess pore water pressure ratio in decimal form, p_R is the soil resistance in Rollins liquefied sand model, y_R is the pile body deflection in Rollins liquefied sand model.

When using Eq. (12), as r_u approaches 0, the calculated soil resistance will be infinitely large. Therefore, this modification method does not apply to soil layers with small r_u.

3. CASE STUDY AND RESULTS DISCUSSION

3.1 The Effect of Excess Pore Water Pressure on Pile Behavior

The analyzing software used in this study is LPILE2013 from Ensoft Inc. It simulates the behaviors of a single pile under pile head loading (axial force, shear force, or moment), or given pile head deflection or rotation. The simulations include the distribution of shear force, moment, soil reaction force, and pile body deflection.

Chang-Hua precursor offshore wind-farm is selected to perform case study (Chien *et al*. 2015). The simplified soil profile of this site is shown in Fig. 3. The soil parameters of this simplified soil profile are listed in Table 1. The following pile head loads, transferring from upper structures, were assumed: Axial force 23,800 kN, shear force 3,910 kN, and moment 21,360 kN-m. A steel pile with the following parameters was installed: Pile diameter D = 2.5 m, wall thickness t = 0.08 m, and length L = 70 m.

Comparison Between API and Reese Sand *p-y* Curve

The typical *p-y* curves at 3 meters suggested by API and Reese were plotted in Fig. 4. The slopes of their initial straight sections and ultimate resistances were almost the same, but the transition curve sections between the two differ a lot. The API *p-y* curve reaches its ultimate resistance at 0.04 m deflection, comparing to 0.09 m of Reese *p-y* curve. A more non-conservative result is obtained using API *p-y* curve. However, in practical practice, pile head deflection and the maximum moment of piles designed with API *p-y* curves are generally acceptable, most engineers still choose API *p-y* curves to reduce cost.

Modification of Excess Pore Water Pressure

In order to compare the differences between the original *p-y* curve and *p-y* curves modified with the two methods, a non-liquefied Reese *et al*. (1974) *p-y* curve and completely liquefied Rollins *et al*. (2005) *p-y* curve were established. *P-y* curves under different r_u were then determined using the modifying methods mentioned above.

Using the case of r_u = 0.5 as an example, the result is plotted in Fig. 5. It can be seen that different types of *p-y* curves were presented for non-liquefied and completely liquefied cases, which are concave-down shape *p-y* curve and concave-up shape *p-y* curve, respectively. There also exists an 8-time difference between their lateral ultimate resistances. The concave-up shape *p-y* curve was caused by:

(1) Under earthquake-induced cyclic loading, small gaps form between soil interfaces will cause the pile body to separate from the soil. From *p-y* curve's point of view, the soil reaction force at the front is zero.

(2) Under pile body large deflection, soil particles around pile body are tightly piling up. Therefore, further increasing of pile body deflection will cause these soil particles to dilate, thus cause the end section of the *p-y* curve to go upward.

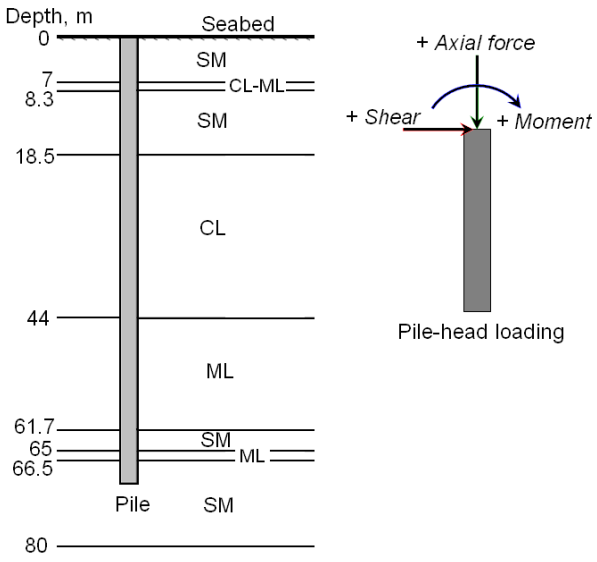

Fig. 3 Simplified soil profile

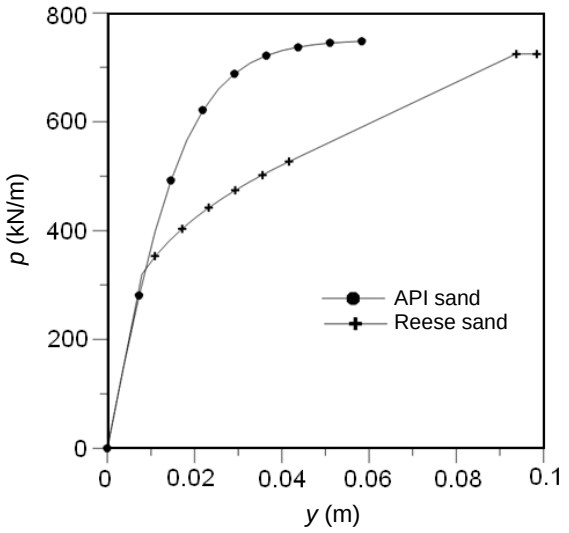

Fig. 4 API and Reese *p-y* curve of sand

Table 1 Soil parameters of simplified soil profile

Depth (m)	Soil type	N	N_{60}	e	ω (%)	γ_t (kN/m^3)	C_c / C_s	c (kPa)	ϕ (deg.)	c' (kPa)	ϕ' (deg.)
0.0 ~ 7.0	SM	2.8	2.7	0.78	25.00	19.1	–	–	–	0.00	31.5
7.0 ~ 8.3	CL-ML	5.0	6.0	0.89	21.00	17.6	–	20.5	0.00	–	–
8.3 ~ 18.5	SM	24.2	30.3	0.62	18.20	19.8	–	–	–	0.00	34.70
18.5 ~ 44.0	CL	10.6	15.4	0.78	27.59	194.	0.32 / 0.034	5.7	20.65	0.00	30.90
4.0 ~ 61.7	ML	18.9	25.2	0.97	34.92	18.8	–	–	–	0.00	35.6
61.7 ~ 65.0	SM	34.5	46.0	0.49	16.00	21.1	–	–	–	0.00	37.4
65.0 ~ 66.5	ML	34.0	45.3	0.52	18.00	20.5	–	–	–	0.00	39.2
66.5 ~ 80.0	SM	30.6	40.7	0.52	17.22	21.0	–	–	–	0.00	36.9

Note: N = SPT-N value, N_{60} = SPT-N value with 60% energy correction, e = void ratio, ω = water content, γ_t = unit weight, C_c = compression index, C_s = swelling index, c = cohesion, ϕ = friction angle, c' = effective cohesion, ϕ' = effective friction angle.

Both modifying methods keep the characteristics of the original *p-y* curves, which are the concave-down shape from Liu and Dobry modifying method and the concave-up shape from Chang and Hutchinson modifying method. When r_u = 0.5, Liu and Dobry method is able to provide 50% of ultimate soil resistance at a lateral deflection of 0.01 m, 0.04 m in the case of Chang and Hutchinson's method.

Deflection Analysis of Pile

This section will compare the effects of different modifying methods and excess pore water pressures on the deflection of pile body. The analysis results were shown in Figs. 6 and 7. Liu and Dobry method was used on Reese sand model in Fig. 6, and Chang and Hutchinson method in Fig. 7.

If Liu and Dobry method is used to modify the Reese sand model, the overall pile deflection tends to be lower (toward non-liquefied side); its pile head deflection only increases by 50% at r_u = 0.7. However, if Chang and Hutchison method is used, a higher (toward liquefy side) overall pile deflection is observed. At r_u = 0.7, the pile body deflection is nearly the deflection amount in the completely liquefied situation.

The relationship between pile head deflection and excess pore water pressure is plotted in Fig. 8. It also compares the cases of Liu and Dobry method with API sand model, Liu and Dobry method with Reese sand model, and Chang and Hutchinson method. The curve of Liu and Dobry with API is about 0.01 m below Liu and Dobry with Reese. When r_u is under 0.2, the pile head deflection obtained from Chang and Hutchinson method is way lower than that of Liu and Dobry method. This phenomenon is caused by the default defect of Chang and Hutchinson method. Therefore, the cases of r_u are not discussed in this study.

From Fig. 8, one can see that all the Liu and Dobry pile head deflections are lower than Chang and Hutchinson pile head deflections. Especially when r_u is greater than 0.4, a 27% difference is observed. Pile head deflection and r_u have a linear relationship in the case of Liu and Dobry method. The pile head deflection in Chang and Hutchinson method case, on the other hand, rise rapidly between r_u = 0.2 and r_u = 0.4, follow by a flatter concave- up curve.

Moment Analysis of Pile

This section discusses the effect of different *p-y* curve modifying methods under different excess pore water pressure ratio on the bending moment distribution of pile. The pile body analysis results of Liu and Dorby on Reese sand model and Chang and Hutchinson methods are shown in Figs. 9 and 10.

From the above figures, one can see that the trend of pile body moment distribution is similar to the trend of pile body deflection, with Chang and Hutchinson method towards liquefying side, and Liu and Dobry method towards the non-liquefy side. The difference is that the depth of the maximum moment increased slowly as r_u increased. It shows in Figs. 9 and 10 that the depth of the maximum bending moment is 7 m when r_u is 0, and 11.9 m as r_u increased to 1.0. As soil liquefied, it becomes soften and the pile deformation increased. Not only will the maximum bending moment increase, the depth of its location increased as well.

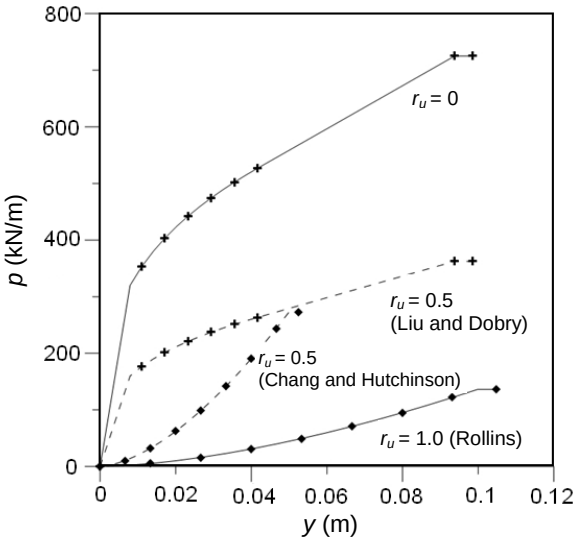

Fig. 5 Comparison between *p-y* curves of the two modifying methods and original base

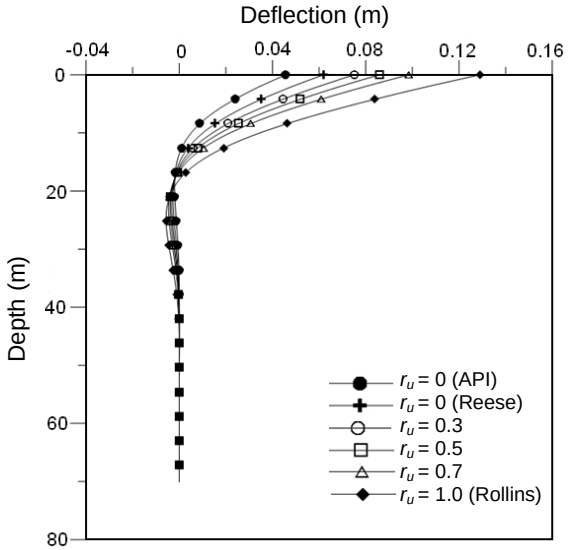

Fig. 6 Pile head deflection of Liu and Dobry method with Reese sand model

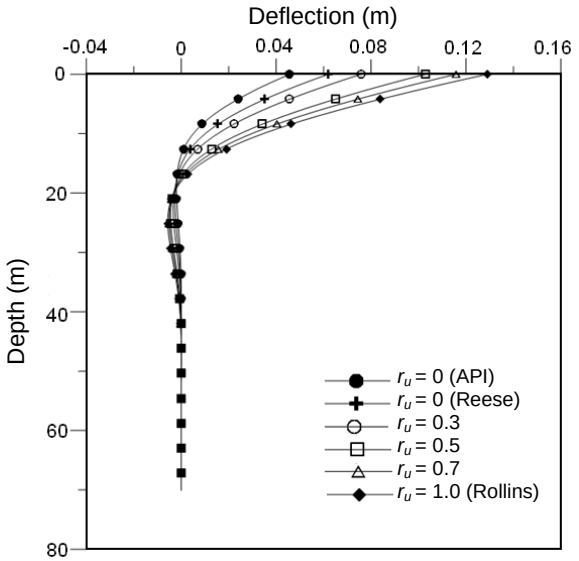

Fig. 7 Pile deflection of Chang and Hutchinson method

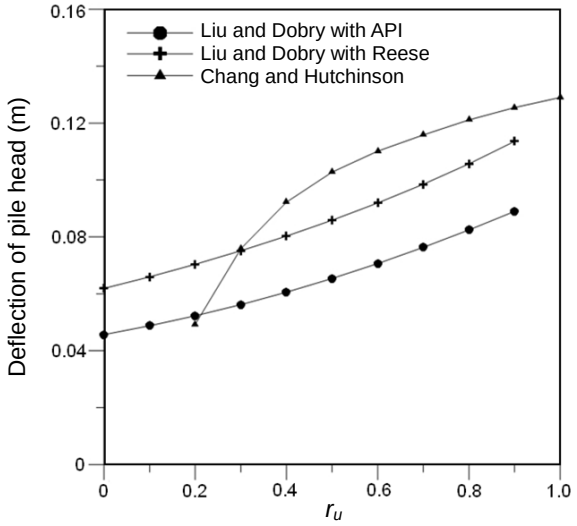

Fig. 8 Relationship between pile head deflection and excess pore water pressure

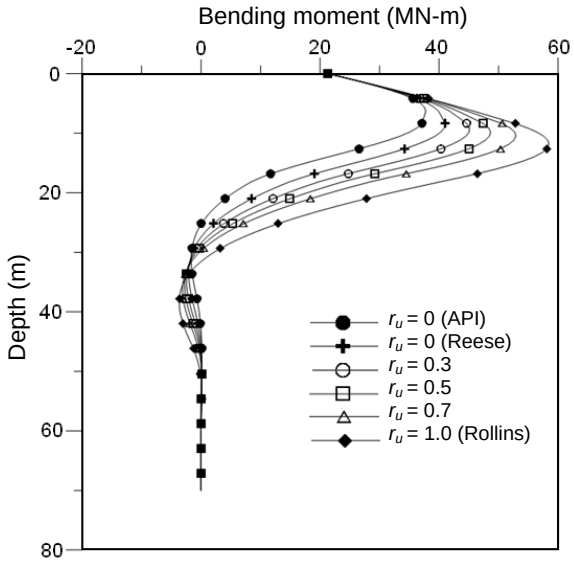

Fig. 9 Pile bending moment of Liu and Dobry method with Reese sand model

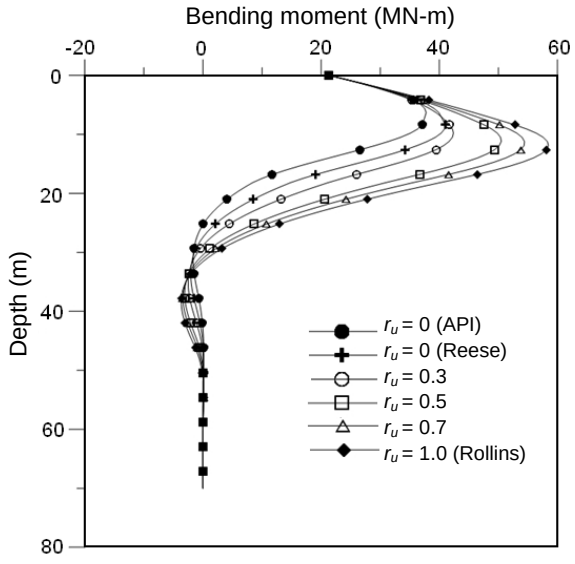

Fig. 10 Pile bending moment of Chang and Hutchinson method

The relationship between the pile body maximum bending moment and excess pore water pressure ratio is plotted in Fig. 11. Three cases are compared, which are Liu and Dobry method with API sand model, Liu and Dobry method with Reese sand model, and Chang and Hutchinson method. The curves of the two Liu and Dorby methods are similar, with the API curve about 2,500 kN-m below the other one. API and Reese sand models also have a smaller impact on the maximum bending moment, in the case of maximum pile head deflection. When r_u is under 0.2, the maximum bending moment of Chang and Hutchinson method is far less than Liu and Dobry method. This is also due to the same default defect of this method. Therefore, the case of r_u being under 0.2 will not be discussed.

As seen in Fig. 11, all the maximum moments obtained using Liu and Dobry methods are lower than that using Chang and Hutchinson method. The maximum moments of Liu and Dobry method increases linearly with r_u, and the maximum moment of Chang and Hutchinson method increases rapidly between $r_u = 0.2$ and 0.4, followed by a flat concave-up curve. As r_u goes over 0.9, the three methods have a similar value.

3.2 Effects of Pile Diameter

Normally, a pile with greater stiffness will have smaller lateral deflection under lateral loading. Therefore, behaviors of pile foundations, including moment, shear, soil reaction force, and rotation angles, will also be affected by its diameter and thickness. If the relationships between physical parameters and mechanics parameters can be found, one can be able to determine the location of the maximum pile head deflection, rotation angle, and plastic hinge to create a safe and economical design. Analysis of the effects of pile diameter on pile behavior under lateral loading at $r_u = 0$ is described below.

In order to simulate the vertical forces, lateral forces, and eccentric moments applied on pile foundations from wave and upper structure of turbine, the concept of combined load and DNV-OS-J101 regulation is used in this analysis. Three factors were discussed in this study including: Axial force (buoyancy force and allowable bearing capacity), combined load (vertical force, lateral force, and moment), and the drivability of the pile. The average loading of each single pile within the group pile was then calculated. The combined loads used in this study are: 23,800 kN vertical force, 3,910 kN lateral force, and 21,360 kN-m moment.

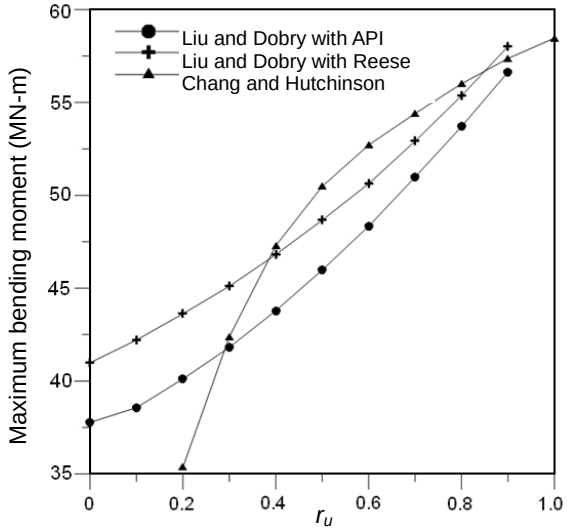

Fig. 11 Relationship between the maximum pile moment and r_u

The type of pile used in this study is open-end steel piles. Dimensions of each single piles are: 70 m total length, 345 MPa yield strength, and 1.8 m, 2.0 m, 2.2 m, 2.5 m, 2.8 m, and 3.0 m pile diameter. The thickness of the single piles is 75 mm at a depth shallower than 20 m, and 50 mm from depth 20 m to 70m. The effect of pile diameter on pile head deflection and rotation angle is discussed.

Deflection, Rotation Angle, and Moment

The flexural stiffness of a pile foundation increased as pile diameter (*D*) and pile wall thickness increased. As shown in Fig. 12, the resulting pile head deflection of the initial design is 0.1443 m, which still meets the regulation. Pile head deflection will decrease to a certain value and remain constant. Under the same loading condition, pile head deflection decreases as pile diameter increased. As seen in Fig. 12, as pile diameters reach 2.8 m and 3 m, the resulting pile head deflections are 0.0387 m and 0.0338 m, respectively, which are about 1.25% of the pile diameter *D*. Moreover, as depth increases, soil stiffness increases as overburden pressure builds up. Thus the pile deflection decreases with the increasing confining pressure. As seen in Fig. 12 again, the critical depth of the pile foundation, where pile deflection is zero, is located at 17 m deep, which agreed with the finding of Reese and Wang (2008). They proposed that the effective range of pile under lateral loading is within 8D deep from the ground surface.

Like pile head deflection, pile head rotation angle decreases as pile diameter increases. As shown in Fig. 13, the rotation angle of the initial design is –0.0185 rad. The negative sign indicates opposite direction from originally defined coordinates, which is counterclockwise in this case. Pile head rotation angle will decrease to a certain value and remain constant. When the pile diameter is 3 m, the pile head rotation angle is 0.003974 rad, and the angle decreases as depth increases. It reaches its critical depth at 25 m. The critical depth of each pile foundation depends on its pile diameter.

Since free end pile head is used in this study, the pile head moment is equal to the applied moment 21,360 kN-m. As shown in Fig. 14, the maximum bending moment of the initial design is 43,513 kN-m. The maximum bending moment decreases as pile diameter increases. However, the depth of where the maximum bending moment occurs does not change with pile diameter. In this case, the location of the maximum bending moment occurs at 7.7 m to 8.4 m.

Pile head deflection, rotation angle, bending moment, and change of stress of different pile diameter were organized and plotted to provide an optimal design that is both safe and economical.

Lateral Load, Pile Head Deflection, and Moment

The single pile horizontal single direction load applying includes five different loads: 1,000 kN, 2,000 kN, 3,000 kN, 4,000 kN, and 5,000 kN, to determine their pile head deflections. The analysis results were plotted in Fig. 15. In the case of 1.8 m diameter single pile, the resulting deflections are 0.01 m, 0.022 m, 0.0383 m, 0.062 m, and 0.095 m, respectively. In practical design of pile foundations, not only the effects of lateral forces, but also the effects of vertical forces and moment, to pile head deflection have to be considered. Pile head deflection increases as lateral load increases, and the increment amount decreases as lateral load increases. In the case of 1.8 m diameter single pile, the curve of lateral force versus pile head deflection is linear when the applied lateral force is less than 2,500 kN. As applied lateral load increases to over 2,500 kN, the curve flattens and become a parabola, which means it is in a plastic state. As pile diameter increases, pile head deflection decreases and the curves move toward left and become a straight line. Soil yield strength also increases as pile diameter increases. For piles with a larger diameter, the lateral forces required to induce pile plastic behavior are also larger. As explained in previous chapters, the plastic behavior of piles not only will induce by load conditions but also pile properties.

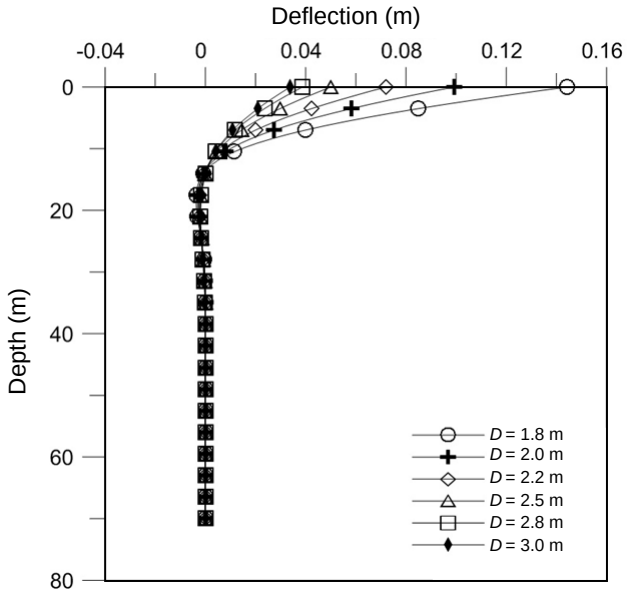

Fig. 12 Relationship between deflection and depth under different pile diameters

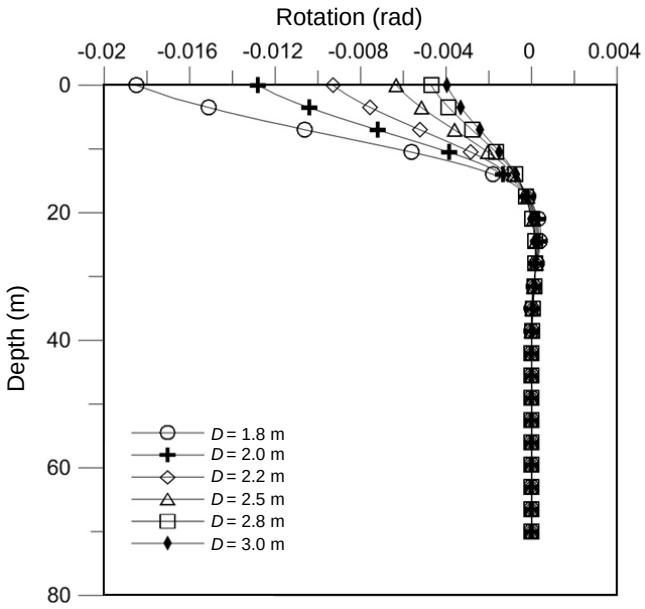

Fig. 13 Relationship between rotation and depth under different pile diameters

The maximum bending moment of single piles under five different lateral loads was plotted in Fig. 16. As applied lateral load increases, the maximum bending moment increases, and as pile diameter increases, the curves move toward the right side and the maximum bending moment increases. In the case of 1.8 m diameter pile, the soil is in elastic condition when the applied lateral load is less than 3,250 kN, and the curves move toward the right as pile diameter increases. However, as applied lateral load goes over 3,250 kN, soil enters into the nonlinear state, and the increment of maximum bending moment decreases. The curve also changes from straight line to parabola after 3,250 kN. The curve of the 2.0 m diameter pile intersects the 2.2 m diameter pile at lateral load = 4,100 kN. The intersection lateral loads increase as pile diameters increase. This shows that as pile diameter increases, the bearable lateral yield force in elastic range increases as well, and the plastic behavior occurs later.

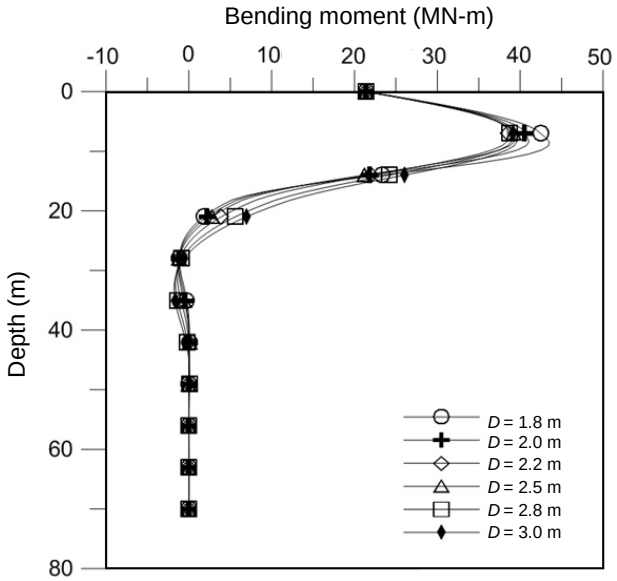

Fig. 14 Relationship between bending moment and depth under different pile diameters

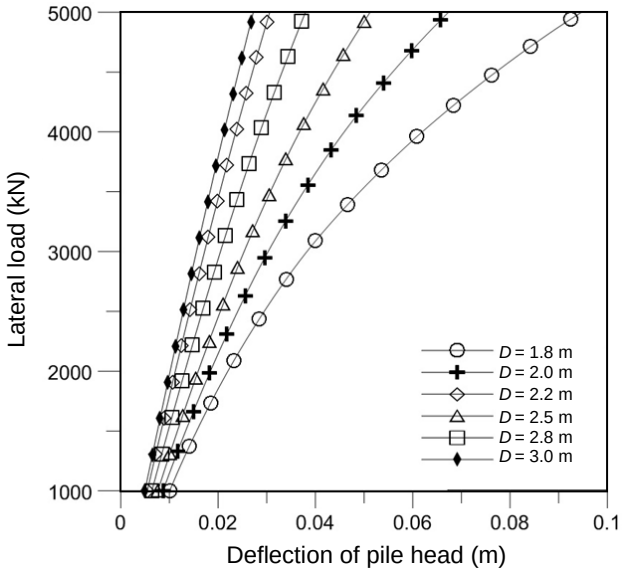

Fig. 15 Relationship between lateral force and pile head deflection under different pile diameters

Summary

A comprehensive summary is made in this section. Since large diameter piles of a diameter larger than 2 m are the most widely used sizes in offshore wind turbine design, pile diameters of 1.8 m to 4 m are analyzed here. As shown from Figs. 17 to 19, pile head deflection, pile head rotation, and the maximum bending stress of pile decrease as pile diameter increases. The regulation requires that the pile head deflection has to be less than 10% of the pile diameter, and the pile head rotation has to be less than 0.005 rad. The software uses these specifications as a threshold to evaluate each design. The initial design, which has a pile diameter of 1.8 m, satisfied the pile head deflection regulation with 0.1443 m deflection. However, it fails the rotation check with 0.0185 rad pile head rotation. From the resulting figures, the optimal design pile diameter is 2.8 m, which satisfied both deflection and rotation regulations.

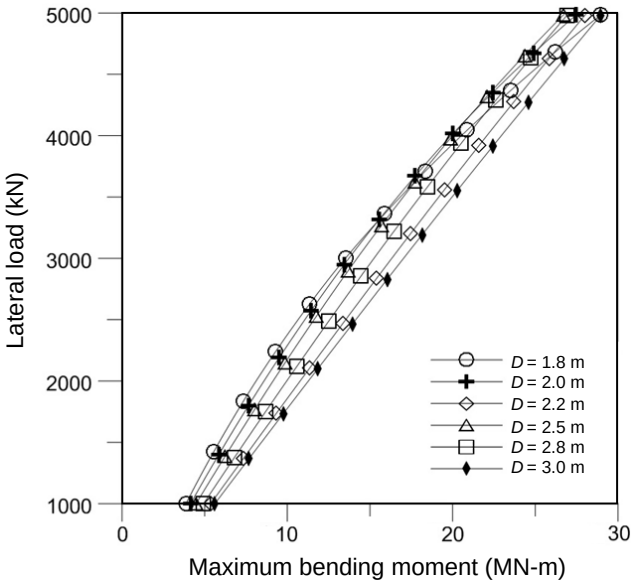

Fig. 16 Relationship between lateral force and the maximum bending moment under different pile diameters

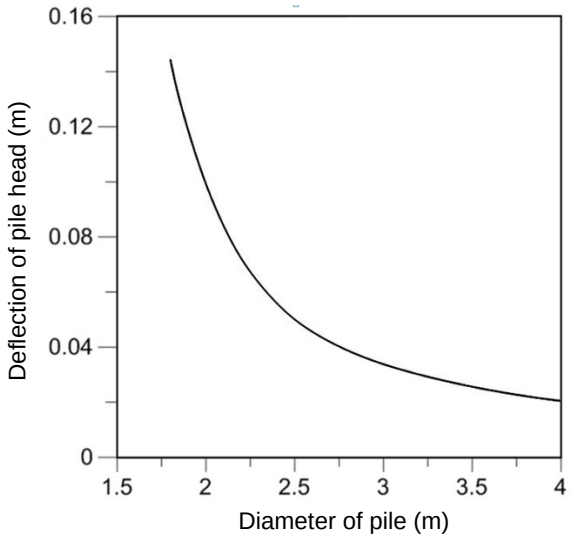

Fig. 17 Relationship between pile head deflection and pile diameter

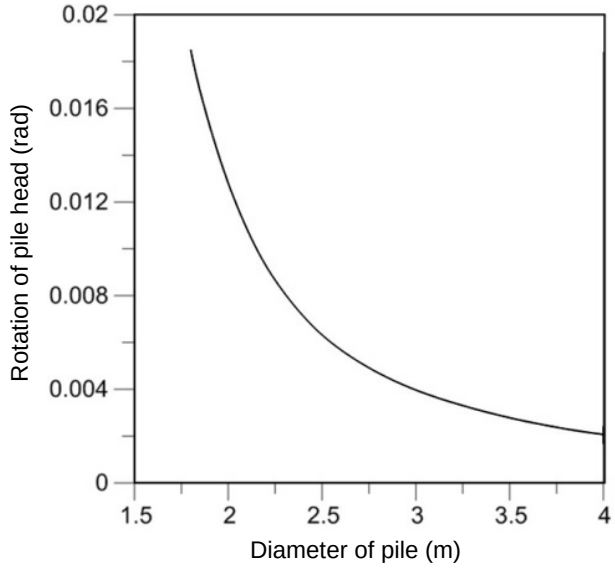

Fig. 18 Relationship between pile head rotation and pile diameter

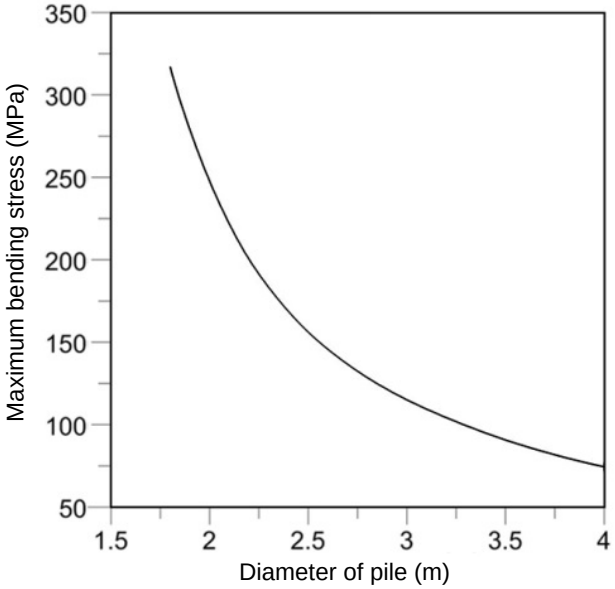

Fig. 19 Relationship between the pile body maximum bending stress and pile diameter

4. CONCLUSIONS

The conclusions from this study can be drawn as follows.

1. The modified results of Liu and Dorby modifying method are in the non-liquefied side because Reese sand model is used as its base. The modified results of Chang and Hutchinson modifying method, on the other hand, are in the completely liquefied side because Rollins sand model is used as its base.
2. The *p-y* curves of partially liquefied soil concaves up, therefore, Chang and Hutchinson modifying method has a more accurate prediction comparing to the modifying method of Liu and Dobry.
3. Chang and Hutchinson modifying method over-amplifies the ultimate soil resistance when r_u is less than 0.2 with a 5-time *p*-value. Therefore, it is suggested that the use of Chang and Hutchinson modifying method is to be avoided when r_u is less than 0.2.
4. When calculating pile head deflection, API sand *p-y* curves produce more conservative results than Reese sand *p-y* curves.
5. The maximum moments of Liu and Dobry modifying method are slightly lower than Chang and Hutchinson modifying method.
6. As lateral load increases, pile head deflection increases, and the increment of pile head deflection decreases. As pile diameter increases, pile head deflection decreases.
7. As lateral load and pile diameter increases, the maximum bending moment increases as well. The bearable yield lateral force in the elastic range also increases. It means that in gets harder to induce plastic behavior.
8. In piles under lateral load at the same depth, in either sand or clay, the exerted soil resistance to reach a certain deflection increases as pile diameter increases.

ACKNOWLEDGEMENTS

The study on which this paper is based was supported in part by the Ministry of Science and Technology, Taiwan, R.O.C. under the grant number MOST 104-3113-E-006-015-CC2. Grateful appreciation is expressed for this support.

REFERENCES

American Petroleum Institute (API) (2005). *Recommended Practice for Planning Designing, and Constructing Fixed Offshore Platforms*. API Report No. 2A-WSD, Houston.

Chang, B.J. and Hutchinson, T.C. (2013). "Experimental evaluation of *p-y* curves considering development of liquefaction." *Journal of Geotechnical and Geoenvironmental Engineering*, ASCE, **139**(4), 577–586.

Chien, L.K., Chiu, S.Y., Feng, Z.W., and Lin, C.K. (2015). "The geotechnical investigation of offshore wind farm for Fuhai development zone." *Sino-Geotechnics*, **142**, 59–68 (in Chinese).

Det Norske Veritas (DNV) (2013). *Design of Offshore Wind Turbine Structures, Offshore Standard DNV-OS-J101*, DNV, Norway.

Ensoft (2013). *Computer Program LPILE v2013 – A Program to Analyze Deep Foundations under Lateral Loading*, Austin, Texas.

International Electrotechnical Commission (IEC) (2009). "Design requirements for offshore wind turbines." *IEC61400-3*, Switzerland.

Japan Road Association (1996), *Design Specifications of Highway Bridges, Part V Seismic Design*, JRA, Japan.

Liu, L. and Dobry, R. (1995). "Effect of liquefaction on lateral response of piles by centrifuge model tests." *NCEER Bulletin*, **9**(1), 7–11.

Murchinson, J.M. and O'Neill, M.W. (1984). "Evaluation of *p-y* relationships in cohesionless soils." *Analysis and Design of Pile Foundations, Proceedings of a Symposium in Conjunction with the ASCE National Convention*, 174–191.

Ni, S.H., Xiao, X., and Yang, Y.Z. (2014). "A *p-y* curve-based approach to analyze pile behavior for liquefied sand under different stress states." *Journal of GeoEngineering*, **9**(3), 85–94.

Reese, L.C., Cox, W.R., and Koop, F.D. (1974). "Analysis of laterally loaded piles in sand." *Proceedings of the Sixth Annual Offshore Technology Conference*, Houston, Texas, OTC 2080, 473–483.

Reese, L.C. and Wang, S.T. (2008). "Design of foundations for a wind turbine employing modern principles." *ASCE Geotechnical Special Publication No. 180 – From Research to Practice in Geotechnical Engineering*, edited by Laier J., Crapps D., and Hussein, M., 351–365.

Rollins, K.M., Gerber, T.M., Dusty, L.J., and Ashford, S.A. (2005). "Lateral resistance of a full-scale pile group in liquefied sand." *Journal of Geotechnical and Geoenvironmental Engineering*, ASCE, **131**(1), 115–125.